Generalized Synthesis of Hybrid Metal–Semiconductor Nanostructures Tunable from the Visible to the Infrared

Bishnu P. Khanal,[†,§] Anshu Pandey,[†,§] Liang Li,[†] Qianglu Lin,[‡] Wan Ki Bae,[†] Hongmei Luo,[‡] Victor I. Klimov,[†] and Jeffrey M. Pietryga[†,*]

[†]Center for Advanced Solar Photophysics, Los Alamos National Laboratory, Los Alamos, New Mexico 87545, United States and [‡]Department of Chemical Engineering, New Mexico State University, Las Cruces, New Mexico 88003, United States. [§]These authors contributed equally to this work.

ABSTRACT

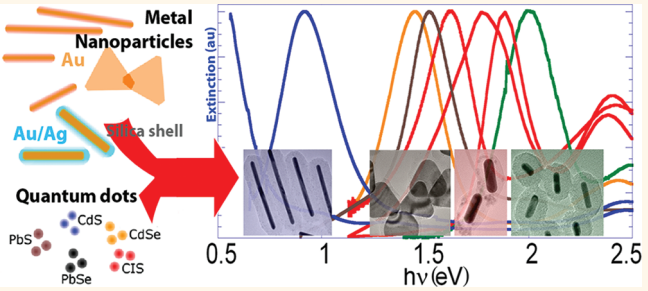

Hybrid superstructures allow a convenient route to the development of materials with multiple functionalities (e.g., sensor, marker, conductor) out of monofunctional (e.g., excitonic, plasmonic) building blocks. This work describes a general synthetic route to the preparation of metal|dielectric|quantum dot hybrid superstructures that have excitonic and plasmonic resonances independently tunable from the ultraviolet to the mid-infrared spectral region. We demonstrate that structural tuning can be used to control intercomponent coupling leading to the emergence of unique optical properties. We illustrate this capability by demonstrating single- and multicolor emission from coupled systems, and a significant enhancement of two-photon absorption cross sections of quantum dots. Such properties in a robust yet dispersible particle can be useful in a number of applications including bioimaging and microscopy, and in optoelectronic devices, as well as serve as a platform for fundamental studies of metal–semiconductor interactions.

KEYWORDS: quantum dots · excitons · metal nanoparticles · plasmons · multifunctional materials · two-photon absorption

Semiconductor nanocrystal quantum dots (NQDs) are a unique class of tunable, dispersible fluorophores of great interest for applications in a wide range of opto-electronic devices. Semiconductor NQDs exhibit large absorption cross sections and can be synthesized to luminesce with high quantum yields from the UV to the mid-IR spectral regions. The push for ever increasing performance in NQD-based devices has made it desirable to go beyond simple control over effective band gap and to introduce influence over more fundamental properties, such as fluorescence lifetimes and absorption cross sections. As an example, while NQDs are excellent fluorophores in the IR, such NQD emission lifetimes can be as long as several microseconds.[1] Enhancement of the radiative rate would allow infrared NQDs to be used in, for example, communication applications. Similarly, enhancement of band edge absorption cross sections of NQDs of indirect-gap materials, such as silicon, can potentially lead to improved light capture efficiencies, potentially benefitting solar cells. The numerous efforts in controlling NQD structure, whether by changing the size or shape, or by introducing heterostructuring, have not shown any potential for significantly enhancing cross-section or radiative rate. Consequently, hybrid metal-NQD materials have received increasing interest as a possible means to tackling these problems.

The processes of light absorption and emission, as well as Förster resonance energy transfer, in NQDs can be significantly affected by proximal metal nanoparticles (NPs) through coupling between NQD excitations and metal surface plasmons (SPs) of metal structures.[2−4] The exploitation of such effects has great potential in lasing,[5,6] solid-state lighting,[7] photovoltaics,[8,9] and sensors.[10−13] However, experimental advances in this direction have been to a great extent phenomenological, as each hybrid material system presents a different measure of control over key parameters that determine the strength of NQD-metal coupling.[14−17] Ideally, a system of truly general value, both for application and for fundamental study, would allow systematic control over a host of material properties, including not only effective band gap and metal–NQD stoichiometry, but also over those parameters determining the strength of exciton–SP interactions, including spectral

* E-mail: pietryga@lanl.gov.

Received for review December 17, 2011 and accepted March 16, 2012.

Published online March 16, 2012
10.1021/nn204932m

overlap of respective resonances and interparticle separation distance.[18−22] Finally, while a number of studies and applications make use of layered or otherwise substrate-cast metal−NQD systems,[23−25] a truly versatile material system would retain the highly valuable dispersibility of the original NQDs without disruption of the properties that dictate the exciton−SP coupling.

Development of a single system meeting these demands, particularly over a large range of energies, remains elusive. Chemical synthesis methods are the most promising methods for producing such complex yet dispersible systems, and there have been a number of recent developments in this area, including in particular facile growth of semiconductor shells onto metal NPs,[2,26] and the opposite case of metal−NP-decorated NQDs[27,28] and semiconductor nanorods.[29,30] While such materials often show enhanced absorption, photoluminescence (PL) is quenched by charge transfer processes due to the direct contact between semiconductor and metal domains. Effective separation can be achieved by attaching NQDs to metal NPs using organic or bioderived linkers.[14,31,32] Such systems have excellent potential as sensors, as coupling-based effects on NQD optical properties can be modulated in response to changes in the rigidity and length of such linkers due to changes in their environment. However, many other applications will require a more robust association that can maintain a fixed separation distance regardless of physical or chemical conditions. A promising structure comprises a larger plasmonic gold NP core and "shell" of single, isolated CdSe NQDs coupled through an intervening layer of silica.[15] While these structures are the first dispersible hybrid system to demonstrate the desired plasmonic influence on emissive excitonic properties, they stop short of demonstrating the wide-ranging tunability that truly drives interest in NQD-based systems. This is likely because these structures were developed before the recent explosion in published methods for producing highly regular shape-controlled metal NPs featuring strong UV-IR SPs, which effectively created a reason to attach NQDs with band gaps significantly distant from the 550 nm SP resonance of spherical gold NPs. As a result, the coupling chemistry presented applies to one combination of Au NP shape, NQD formulation (relatively robust CdSe), and solvent, and is not widely applicable to other combinations. In contrast, the methods reported in this work enable us to produce structures of nearly any formulation, including most importantly the attachment of NQDs of less chemically robust materials such as lead chalcogenides or ternary compounds, enabling the synthesis of hybrids with resonances well into the IR.

Here we describe a general method for the chemical synthesis of dispersible metal|silica(SiO_2)|NQD hybrid superstructures with straightforward control over metal NP shape size, NQD composition and loading, and the separation distance (Figure 1). Importantly, we demonstrate the ability to leverage essentially any of the established methods for preparation of NQDs of numerous formulations that offer excellent control over shape, size, and internal structure, and consequently fine control over excitonic properties.[33] Likewise, we take advantage of the incredible selection of shape-controlled metal NPs, whose SP resonances, collectively, cover an energy range that at least matches that of NQDs.[34] To fully exploit this inherent flexibility, NQDs and metal NPs must, as in the previous example,[15] be grown under their own respective ideal conditions. Then, shell-growth and coupling must be performed in a manner that retains the desired optical properties of each, regardless of respective formulation. In the case of metal NPs, this means retention of size and shape; however to retain the properties of the NQD, particularly PL, it is also necessary to avoid damaging the particle surfaces. For chemical reasons, this is especially challenging. The highest quality NQDs are usually grown in nonpolar organic solutions, and display a wide range of surface sensitivies/reactivities depending both on formulation and the identity of the ligands. Contrastingly, metal NPs are grown in a highly polar aqueous solution, while finely controlled silica deposition is best performed in water/alcohol solutions at high pH (>10). As a result, solubilities and residual reactivities must be considered at every step of the way.

Our flexible approach enables the creation of hybrid superstructures with enhanced optical properties, including record high two-photon absorption cross sections and new functionality such as multicolor (potentially "white-light") emission, tunable from the visible to the mid-IR. Such properties tunable over such a broad energy range could potentially benefit several optical and optoelectronic applications including NQD-based sensing, microscopy and imaging, light emitting diodes as well as photodiodes and photovoltaics. In addition to the potential for modifying the emission characteristics of the NQD chromophores, these hybrid structures may offer unique properties through their independently accessible plasmonic/excitonic bifunctionality. Thus, for example, the same structure may be utilized for PL imaging as well as for sensing local molecular environments through surface-enhanced Raman scattering.

RESULTS AND DISCUSSION

In a typical synthesis we construct a hybrid nanostructure based on single-crystalline gold nanorods (AuNRs) that demonstrate strong longitudinal SP features ranging from the visible into the IR, depending on the aspect ratio. AuNRs with a longitudinal SP near 800 nm are synthesized using a seed-mediated growth method developed by Murphy, *et al.*,[35] and later modified by El-Sayed, *et al.*[36] After careful and thorough removal of excess cetyltrimethylammonium

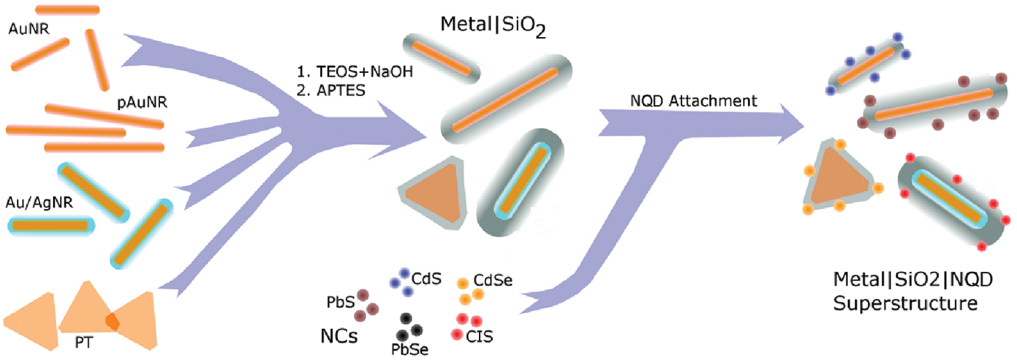

Figure 1. A single, generalized reaction pathway can be used to fabricate hybrid superstructures with enhanced optical properties over a large energy range. Shape-controlled Au NPs can exhibit SP resonances tunable from the UV to the mid-IR, equivalent to the collective range of excitonic energies covered by NQDs of only a handful of formulations. A slow base-catalyzed hydrolysis reaction is employed to overgrow a porous silica shell that is further activated with either amine or thiol functions. Following this, NQDs may be decorated with the structure to form the metal−silica−NQD hybrid.

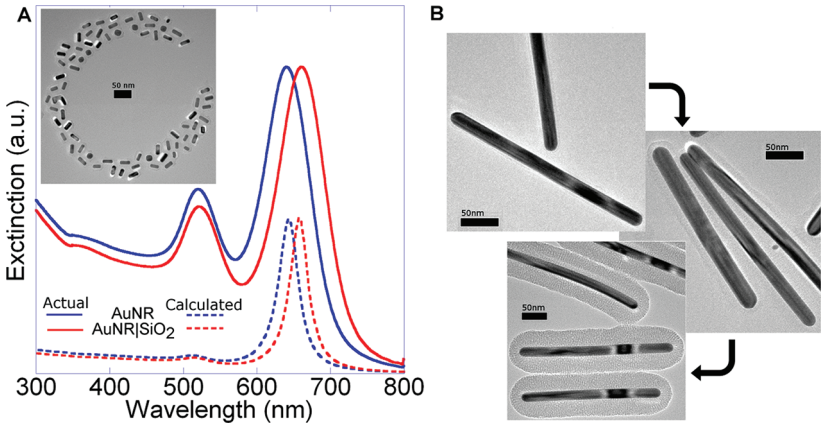

Figure 2. (A) Extinction spectra of a AuNR sample before and after coating with 10 nm of SiO_2. Spectra have been normalized to the longitudinal SP. The dashed lines represent calculated spectra. Inset: self-assembly of the silica-coated nanorods on a TEM grid. (B) TEM images showing progressive growth of the SiO_2 shell.

bromide (CTAB) surfactant, the NRs can be coated with a 4−30 nm thick shell of silica *via* a slight modification of a previously reported procedure.[37,38] Specifically, a slow, base-catalyzed hydrolysis (over 48 h) of tetraethylorthosilicate (TEOS) in methanol results in a uniform, continuous silica coating without the formation of free silica spheres and with no effect on Au NP shape or size discernible by transmission electron microscopy (TEM). The thickness of the silica layer can be controlled by increasing or decreasing the amount of TEOS and NaOH, or through subsequent iteration of the entire process. As shown in Figure 2A, the longitudinal SP shifts toward longer wavelengths (up to 20 nm for 10 nm of shell) due to the higher dielectric constant of the silica shell. After measuring the silica thickness of a number of rods by TEM, the rod and the silica shell were modeled as ellipsoids in the electrostatic approximation to extract the effective dielectric constant of the silica shell, which is estimated to be ∼2.09.[39,40] Assuming that the shell dielectric varies linearly between the dielectric constant of pure silica (2.13) and the solvent (1.78 for water), the optical redshift of the longitudinal rod SP suggests that the shell is dominantly solid silica, with *ca.* 10% of its volume taken up by water included during growth. Assuming a reasonable distribution of water throughout the shell volume, this essentially precludes the formation of any surface-accessible pores large enough to accommodate organic-functionalized NQDs. Thus, this impenetrable silica shell establishes a tunable, yet fixed and consistent separation distance between the metal NP and the NQDs in the final superstructure. In addition to the redshift of the longitudinal SP resonance, its extinction cross section is also increased by ∼25% relative to the transverse feature. The response of the transverse feature to changes in the dielectric environment is smaller because of the larger contribution to its overall intensity from interband absorption. These spectral changes can be used to monitor the progress of reaction for fine thickness control; when the desired thickness is reached, the silica-coated NPs are removed from the solution by centrifugation and redispersed in pure ethanol.

To create a superstructure that can be expected to maintain its metal:NQD ratio in a variety of environments, it is desirable to attach NQDs by direct chemical bonds of the type found between the NQD surfaces and their passivating ligands, rather than relying simply on electrostatically induced aggregation. Thus, in advance of

introducing NQDs, the Au|SiO_2 NRs in ethanol are functionalized by addition of 3-aminoproplytriethoxysilane (APTES) with stirring, and again purified by centrifugation/redispersion. The NQDs to be attached, for example, colloidal PbS/CdS NQDs,[41] are then introduced as a THF solution to the NR solution dropwise with vigorous stirring. To maximize attachment of NQDs to the functionalized Au|SiO_2 surface, excess ligands and weakly associated organics were removed from the NQDs thoroughly by repeated cycles of precipitation (by addition of a short chain alcohol such as ethanol or propanol, *etc.*) and redispersion in toluene before finally dispersing in THF. Partial substitution of NQD surfactants by a more labile surfactant such as octadecylamine or trioctylamine, prior to introduction to the silica-coated metal, was found to lead to more efficient attachment in the case of Cd- and Zn-based NQDs. The pendant amine functionalities presented by the "activated" silica surface displace surfactants on the NQD surfaces, resulting in a robust linkage. The hybrid AuNR|SiO_2|NQD superstructures are then purified from excess, unbound NQDs by centrifugation and redispersion in THF. Use of an excess of NQDs results in reproducible and uniform loading on the SiO_2 surface; lower loading levels (*i.e.*, number of NQDs per AuNR) can be achieved without loss of uniformity by reducing the relative amount of APTES used during functionalization. As anticipated considering the essentially nonporous silica layer, the NQDs are able to attach only to the outer surface of the shell, meaning that all NQDs reside at a well-defined distance from the central AuNR.

The retention of PL for most NQD formulations proved to be nontrivial, and required substantial experimentation with synthesis conditions. There is some evidence that residual reactivity from incomplete hydrolysis within the silica shell has deleterious effects on the PL of attached NQDs. Universally, the pretreatment of APTES-functionalized Au|SiO_2 structures by a weak acid such as ascorbic acid was found to improve PL quantum yields of the final superstructures relative to the quantum yields observed in the case of untreated structures, implying that the responsible reactive sites are basic in nature. Finally, it is important to mention that while the solubility of Au|SiO_2 nanostructures is higher in THF, the oxidizing environment presented by peroxides in unstabilized THF was also found to be detrimental to the PL of a number of core-only NQDs as well as NQDs with thin inorganic shells, both before and after attachment. In fact, Au/Ag core/shell bimetallic NRs were also prone to oxidation under these conditions. Ascorbic acid, as an antioxidant, can help prolong NQD stability in THF with low levels of peroxides, but not indefinitely. For these reasons, it is often advisable to use chloroform as the solvent.

The technique described above is extremely general and may be reproducibly applied to a variety of metal nanostructures and NQDs, with strikingly different chemistries, to produce superstructures in which both the SP and exciton resonances may be independently

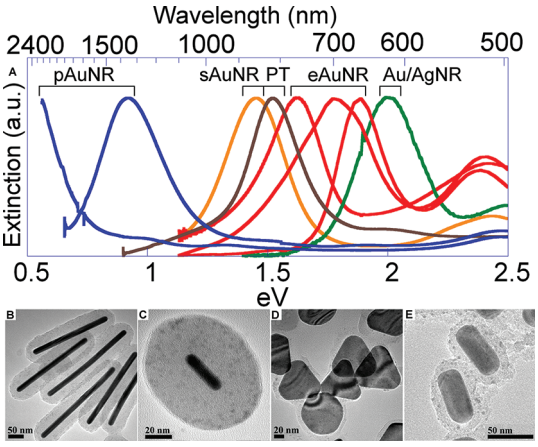

Figure 3. (A) Extinction spectra of various SiO_2-coated metal nanostructures. From lower to higher energy: pentahedrally twinned AuNR (pAuNR); single-crystalline AuNR (sAuNR); Au platelets (PT); etched AuNR (eAuNR); and silver-coated AuNR (Au/AgNR). (B–E) TEM images of various superstructures: (B) pAuNR|SiO_2|CdSe/ZnS, (C) sAuNR|SiO_2|PbS, (D) platelet|SiO_2|-CdSe/ZnS, (E) Au/Ag NR|SiO_2|CdSe/ZnS).

tuned from the visible to the mid-IR region by varying the shape of the metal NP (Figure 3) and the composition and size of the NQD.[42−45] As-synthesized AuNRs have an aspect ratio of 3:1, which produces a longitudinal SP resonance at 800 nm. This resonance may be tuned into the visible region either by reducing the aspect ratio, or by overcoating the AuNR with silver (Ag).[34] Reduction of the aspect ratio by selective etching[46] of the nanorod tips is accomplished by treatment of the NRs with an Au^{3+}/CTAB solution, which preferentially oxidizes Au atoms at the highly curved rod tips, where the CTAB coverage is less dense, leading to the formation and dissolution of Au^{1+} ions.[47] The reaction may be stopped once the desired spectral position of the gold SP is reached by removal of the AuNRs from the Au^{3+}-rich solution *via* centrifugation. Alternatively, the tuning of the SP across the visible spectrum may also be accomplished by overcoating AuNRs with Ag using a variation of a published method.[34] Either technique allows fine, reproducible tuning of the longitudinal SP resonance at the ~10 nm level, and results in particles fully amenable to subsequent inclusion in hybrid superstructures.

Superstructures may be prepared on Au NPs of completely different structural motifs as well. Two relatively new examples include pentahedrally twinned AuNRs (pAuNRs, Figure 3B) and quasi-2D Au platelets (Figure 3D). pAuNRs can exhibit very large aspect ratios and corresponding longitudinal SP features extending into the mid-IR energies while platelets have a surprisingly narrow feature in the near-IR that is largely insensitive to the degree of faceting. These shapes are synthesized simultaneously in a mixture (~9:1 platelets:NRs) by a previously reported method, and isolated *via* a highly selective procedure developed recently by Zubarev and co-workers.[47,48] Once isolated,

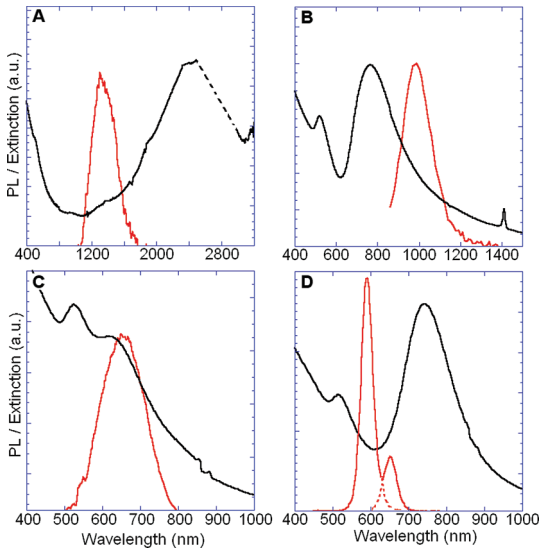

Figure 4. Absorption (black) and PL (red) spectra for superstructures over a wide range of energies. (A) pAuNR| PbSe/CdSe. The structure extinction spectrum in the 2400−2800 nm region (dashed line) is obscured by the solvent; (B) sAuNR|SiO_2|PbS/CdS; (C) eAuNR|SiO_2|CIS/CdS; (D) dual emissive superstructure with CdSe/ZnS NQDs of two different sizes on a sAuNR. The dashed lines represent PL spectra of the individual components. Variations in emission intensities between individual superstructures, and between different NQDs within the same superstructure (as in D), reflect relative loading levels (*i.e.*, number of NQDs per metal NP).

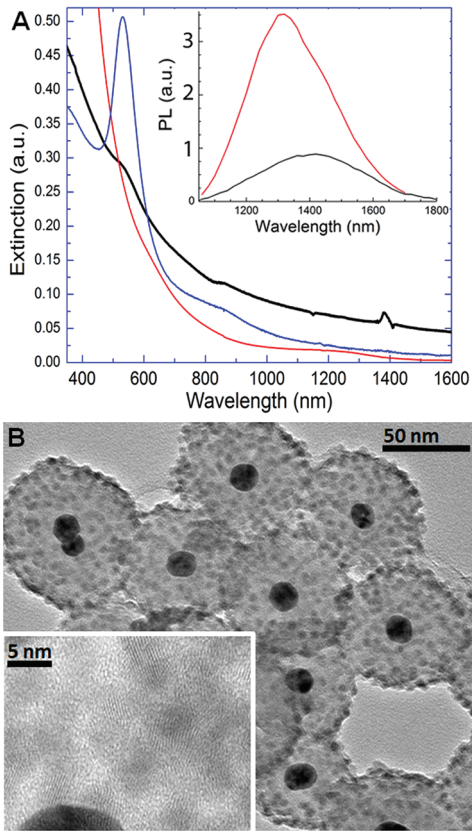

Figure 5. (A) The absorption spectra of PbSe/CdSe NQDs (red), Au NPs with 20 nm SiO_2 shells (blue) and the product superstructure after attachment (black), arbitrarily scaled for clarity. Inset: PL of the NQDs before (red) and after (black) attachment. The red shift is likely a sign of NQD−NQD energy transfer due to the extremely dense loading. (B) TEM image of the superstructures; inset, high-magnification showing NQD lattice fringes.

particles of either shape are further tunable by methods similar to those described above for normal AuNRs. Despite their significantly larger size, superstructures based on either shape may be readily dispersed in ethanol or THF provided the thickness of silica layer is at least ~12 nm, even in the case of pAuNRs that are up to ~300 × 20 nm in size.

To match the variety shown by the metal NPs, the NQD excitonic position may be fine-tuned by varying size, or more coarsely tuned by varying the NQD material. To date, we have successfully used cores and core−shell structures based on CdS, CdSe, $CuInS_2$ (CIS), PbS and PbSe.[41] This enables the preparation of superstructures where the excitonic component, like the plasmonic, may have an energy ranging from the UV (CdS) to the mid-IR (PbS, PbSe) region of the spectrum. In each case, the absorption spectrum is dominated by the metal structure due to its larger cross section, while PL arises from the NQDs. The wide tunability as well as the diversity of these hybrid superstructures is shown in Figure 4. By attaching NQDs of different compositions (PbSe/CdSe Figure 4A, PbS/CdS Figure 4B, and CIS/CdS Figure 4C) to Au nanostructures of appropriate shapes and aspect ratios, a wide spectral range relevant for a variety of applications may be effectively covered. Interestingly this technique also provides a simple route toward achieving multicolor emitting nanostructures. As an example, we synthesize two-color emitting structures by attaching two different sizes of CdSe/ZnS NQDs onto the same AuNR simultaneously. The relative amplitudes of the two PL emission bands may be controlled by varying relative concentrations of the two NQDs in solution. For two different compositions of NQDs, a more accurate control over the superstructure emission may be realized by initially attaching one class of NQD, followed by purification and subsequent attachment of the other NQD.

The structures shown in this initial synthetic study have relatively thick SiO_2 shells, and so generally fall within the regime of weak NP-NQD coupling. Although synthesis of thinner-shell systems with strong coupling is easily accomplished *via* the same methods, the complexity of NP-NQD interactions in these cases creates a large parameter space that we will explore in further studies, each of which will focus on a more limited range of materials. However, because of the sensitivity of PL quantum yields to modification of NQD surface environments, it is important to establish to what extent emission efficiency is diminished in the final superstructures. This is highly complicated by the relatively high absorption cross sections of the metal particles compared to the NQDs, and by the possibility of SP-based enhancement or quenching.

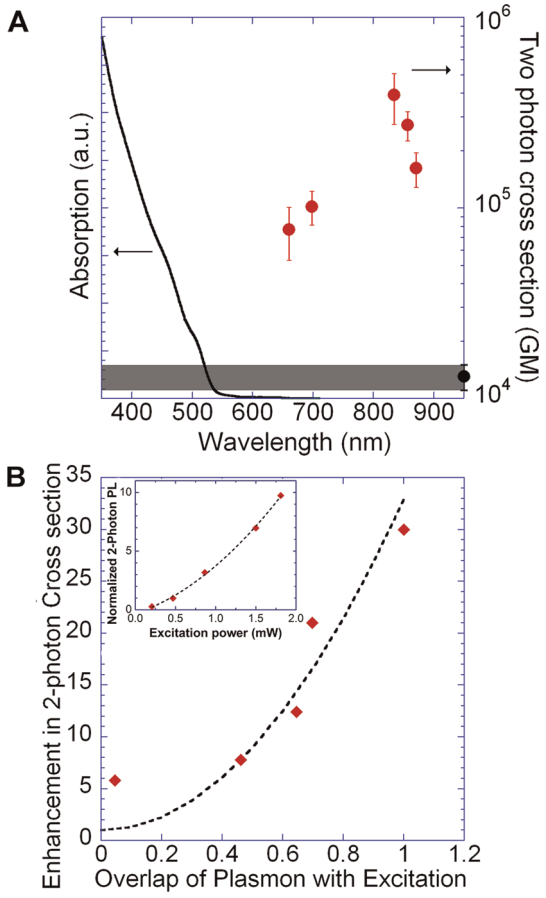

Figure 6. (A) The two-photon absorption cross sections of a CdS/CdSe/CdS/ZnS NQD are significantly enhanced upon inclusion in a AuNR-based superstructure, depending on its SP peak (which reflects aspect ratio). The bare NQD absorption (black line) and two-photon cross section at 800 nm (gray rectangle) are compared to the cross sections for various AuNR|SiO_2|NQD structures, plotted against the SP peak position (red circles). (B) The enhancement of the two-photon cross section increases with the square of the SP-excitation overlap, which in this case is the amplitude of the peak-intensity-normalized longitudinal SP feature at 800 nm. The dashed line is a square fit. Inset: the two-photon PL for a single sample depends quadratically (dashed line) on the 800 nm excitation power (red).

To minimize these effects, we studied a structure which combined a 20 nm spherical Au NP (SP peak at 530 nm), a 25 nm-thick SiO_2 shell, and a heavy loading of 4 nm PbSe/CdS core/shell NQDs (PL peak at 1350 nm). This extreme spacing and spectral separation reduces the chance for coupling effects on PL efficiency to essentially nil. Careful measurement of PL before and after attachment, while accounting for the still quite substantial Au absorption tail into the IR, demonstrates that we can consistently retain at least 30% of the original quantum yield (Figure 5A inset). Batch-to-batch variation and studies using structures based on other NQDs suggest that refinement of the attachment process (*e.g.*, finer control over ligand exchange and APTES functionalization, better solvent quality, *etc.*) can improve this further, likely to the point where substantially more than half of the quantum yield can be preserved.

Interestingly, even in the weak-coupling limit in which linear properties are largely unperturbed, it is possible to still observe large changes in nonlinear optical properties.[49] Dispersible NQDs have been previously noted to exhibit two-photon absorption cross sections orders of magnitude larger than even the most efficient organic dyes currently in use,[50] and thus are of great interest for bioimaging applications such as two-photon excitation microscopy,[51] and for three-dimensional display technologies.[52] We synthesized superstructures in which highly luminescent CdS/CdSe/CdS/ZnS[44] NQDs (chosen for their tunability as well as excellent chemical and photochemical stability) with emission at ~530 nm were coupled to AuNRs of a range of aspect ratios with a 15 nm SiO_2 spacer layer. It is expected that the field enhancement due to the AuNR SP resonance can enhance the effective two-photon cross sections of the NQDs located around the AuNR. Two-photon absorption cross sections were measured by exciting the samples using 250 fs pulsed 800 nm laser. The sample PL was collected at different power levels for 800 nm light, and compared to the PL emission obtained from linear 400 nm photo excitation. Figure 6A demonstrates that coupling of the NQDs to the AuNR has a very significant effect on the two-photon cross sections with the values measured at 800 nm being greatly enhanced relative to the already large value of the original bare NQDs. In testament to the importance of fine-tuning, this enhancement increases from 5- to 30-fold as the AuNR SP is tuned over the excitation wavelength, reaching as high as 4×10^5 GM, surpassing the highest previously reported value, achieved in CdS NRs.[53] Even higher enhancement factors should be achievable through optimization of the silica-layer thickness, which is a key parameter in the strength of the NQD–metal interaction. Figure 6B illustrates the role of the metal SP in the attainment of this result. Assuming the scattering cross sections at the longitudinal SP for all the metal NRs to be similar, the field enhancement of 800 nm light in the vicinity of the metal NR is a linear function of the spectral overlap between the NR SP and the laser excitation. We observe that the enhancement in two-photon cross sections is related to the square of the spectral overlap as is expected from a purely field enhancement point of view.

CONCLUSIONS

The structural motif presented in this study represents a powerful and flexible system for probing the fine details of, and exploiting the interactions between, coupled plasmonic NPs and excitonic NQDs. The ability to combine, at controllable ratio and distance, NQDs and metal NPs of arbitrary formulation, size, and shape allows one to leverage decades of advancement in synthetic control over such properties to arrive at superstructures in which the coupling can be modified on a previously unavailable level of fineness, over an unmatched total

range of energies. Single-crystal AuNRs, pentahedrally twinned AuNRs, Au Platelets and the Au/Ag core/shell rods, when matched with the diverse NQD compositions included in this study, afford a continuously variable system that spans an energy space from the UV all the way into the mid-IR. While only scratching the surface of this potential, this study has already demonstrated several novel properties of large general interest, including the addition of a PL signal to a strongly absorbing metal-NP system; multicolor, potentially white-light emission from single dispersible entities; and record-high two-photon absorption cross sections (which can be used to excite single- or multicolor emission in suitably constructed superstructures). Importantly, once synthesized, these robust hybrid structures can retain their desired coupling properties under diverse conditions, from solution-phase to cast-film, and potentially even while embedded in a variety of matrices, according to the needs of a given study or application. Thus, this single system is potentially relevant to applications from LEDs and displays, to tissue-transparent biomarkers, to solar cells and IR detectors.

METHODS

General Synthesis Details. Hydrogen tetrachloroaurate trihydrate ($HAuCl_4 \cdot 3H_2O$) (99%), cetyltrimethlyammonium bromide (CTAB) (99+ %), and sodium borohydride ($NaBH_4$) (98%) were purchased from Acros Organics. Ascorbic acid (99.7%), sodium hydroxide, anhydrous ethanol, and tetrahydrofuran (THF) (99.9%) were purchased from Fisher Scientific. Silver nitrate (99.99%), tetraethylorhtosilicate (TEOS) (99.95%), and 3-aminopropyl triethoxysilane (APTES) (99%) were purchased from Sigma-Aldrich. DI water was used throughout the experiment. All chemicals were used without further purification. Metal particles were synthesized using modifications of known synthetic techniques.

Seed-Mediated Synthesis of Single-Crystalline AuNRs. *Seed Solution.* In a 40 mL glass vial, $HAuCl_4 \cdot 3H_2O$ (1.97 mg) and CTAB (364 mg) are dissolved in 500 mL of water in 10 mL of water at 25 °C. Ice-cold $NaBH_4$ solution (0.01M, 0.6 mL) is added with vigorous stirring, resulting in the formation of 3−4 nm spherical Au seed particles.

Growth. In a 1000 mL flask, CTAB (18.2 g) and $HAuCl_4 \cdot 3H_2O$ (98.5 mg) are dissolved in 500 mL of water at 25 °C. Aqueous $AgNO_3$ (4×10^{-3} M, 12.5 mL) is introduced and the flask is stoppered and shaken by hand. Next, aqueous ascorbic acid (0.0788 M, 3.5 mL) is added with additional shaking. The reduction of Au^{3+} to Au^{1+} results in the disappearance of dark yellow color. Quickly, 0.8 mL of seed solution is added to the colorless growth solution and shaken. Within 10−20 min the solution becomes reddish brown, indicating the formation of AuNRs. The flask is left undisturbed for 2 h, after which the product NRs are precipitated by centrifugation. For further experiments, the supernatant containing unreacted Au ions is discarded and the AuNRs are redispersed in the desired solvent.

Tip-Selective Oxidative Etching. In a typical experiment, 10 mL of aqueous solution containing 4 mg of $HAuCl_4 \cdot 3H_2O$ and 364 mg of CTAB is introduced into 200 mL of as-synthesized AuNRs solution with vigorous stirring. The evolution of the aspect ratio is monitored by UV−vis spectroscopy, and the reaction is stopped at the desired SP position by centrifugation and removal of unreacted Au^{3+}/CTAB complex.

Seed-Mediated Synthesis of p-AuNRs and Platelets. *Seed Solution.* In a 40 mL glass vial, 1.97 mg of $HAuCl_4 \cdot 3H_2O$ and 1.47 mg of sodium citrate are dissolved in 20 mL of water. $NaBH_4$ solution (0.1 M, 0.6 mL) is added, and the mixture is stirred vigorously. The formation of 3−4 nm spherical gold seed particles is accompanied by a change in the color of the solution from light yellow to brown.

Growth. For clarity, three flasks are labeled A, B, and C. In each flask, 4.72 mg of $HAuCl_4 \cdot 3H_2O$ and 1.82 g of cetyltrimethylammonium bromide (CTAB) are dissolved in 50 mL of water at 25 °C. Aqueous ascorbic acid (0.1 M, 0.5 mL) is added into each flask and hand shaken, whereupon the solutions become colorless. Then, 5 mL of the seed solution is added to flask A with stirring. Within 10 s, 5 mL of solution from flask A is transferred into flask B and hand-shaken for 10 s. Next, 5 mL of solution from flask B is transferred into flask C with stirring. This method produces a mixture of three major shapes- pAuNRs, platelets, and spherical particles. For the separation of pAuNRs from mixtures of shapes, flask C was left undisturbed for 24 h. Most of the pAuNRs and platelets precipitate to the bottom of flask. The supernatant containing mainly spherical NPs is discarded, and the precipitate is redispersed in 10 mL of 0.1 M CTAB solution. The separation of pAuNRs from platelets was carried out by partial oxidation with $HAuCl_4 \cdot 3H_2O$. Partial oxidative etching transforms platelets into circular disks that have relatively higher solubility due to a larger surface area than the pAuNRs, which will selectively precipitate from the undisturbed solution over 24 h. After removal, the disks remaining in the supernatant can be converted back to platelets by regrowing with Au^{1+} solution. The pAuNRs and platelets thus isolated were dissolved in 15 mL of water and used for further experiments.

Synthesis of Au/Ag Bimetallic NRs. The synthesis of Au/Ag NRs is carried out by the chemical reduction of Ag^{1+} ions on presynthesized AuNRs. In a typical experiment, the AuNRs precipitated from a 100 mL portion of the as-synthesized solution prepared above are redispersed in 0.1 M aqueous CTAB solution at 25 °C. To this solution 4.25 mg of $AgNO_3$ is added. Next, aqueous sodium ascorbate (0.1 M, 0.5 mL) and NaOH (0.1M, 0.5 mL) are added simultaneously. The reaction produces an immediate color change from brown to green; the progress of Ag deposition can be monitored by UV−vis spectroscopy, and the reaction can be stopped by centrifugation and redispersion into CTAB/H_2O solution.

Silica Coating of Metal NPs. Silica coating on the surface of AuNRs, pAuNRs, Au nanoplatelets, or Au/Ag bimetallic NRs is carried out by a modified sol−gel method. To 30 mL of NP solution (containing roughly 10^{-11} moles of NPs), 50 μL of 0.1 M NaOH solution are added dropwise with stirring. After 5 min, 50 μL of 20% TEOS in MeOH (by volume) is also added dropwise with stirring. This process is repeated every 8−12 h for up to four total additions, and after the final addition, the solution is stirred for an additional 12 h. These amounts typically result in a 12−15 nm coating of silica, but the amount of TEOS and NaOH used can be varied to modify the thickness of silica layer. The silica-coated NPs are isolated by centrifugation and redispersed in 30 mL of EtOH.

Coupling of NQDs to Silica-Coated Metal NPs. Activation of silica surfaces is accomplished by the addition of 3-aminopropyl triethoxysilane (APTES). In a typical experiment, 100 μL of APTES are added dropwise to the above-prepared 30 mL of an EtOH solution of Au/SiO_2 NPs with stirring. After stirring for an additional 12 h, the activated NPs are isolated by centrifugation and redispersed in 30 mL of tetrahydrofuran (THF). In a typical attachment reaction, 10^{-12} moles of coated Au NPs were mixed with 10^{-9} moles of NQDs in 5 mL of solvent, where concentration is estimated by measuring the optical absorption. The addition of NQDs was performed dropwise with vigorous stirring.

The efficiency of attachment is a strong function of the NQD composition, details of surface coverage and cleaning, the solvent used, and the ligand chemistry. For instance, attachment can be nearly quantitative for amine-capped NQDs in THF, whereas it can be much lower for NQDs featuring other capping ligands. The efficiency of attachment of NQDs may be improved by exchanging the native NQD ligands with more labile ligands

such as trioctylamine or octadecylamine. This step is performed by gently warming the NQDs in a concentrated solution of the chosen amine in toluene to ~40 °C for 5 min. The NQDs are then precipitated and redissolved in toluene at least twice and then finally redispersed in THF. After stirring for an additional 12 h, the components are separated by centrifugation. The supernatant, which mainly contains unattached NQDs, was removed, and the precipitate was redispersed in THF, occasionally assisted by gentle sonication.

To aid in the neutralization of any remaining basic sites from incomplete hydrolysis during silica-shell growth, the THF used in these steps is saturated in a weak acid, such as ascorbic acid, by stirring over an excess of the acid overnight at room temperature. When NQDs that are particularly susceptible to oxidation are used, such as CIS and lead chalcogenide NQDs, THF can be replaced by chloroform in all of the above steps. In chloroform, the attachment efficiency is generally lower than in THF, and so it is particularly important to perform octadecylamine-substitution of the native ligands to increase the attachment efficiency.

Two-Photon Cross Sections. The two-photon absorption cross section was determined by comparing PL intensity from NQD and AuNR/NQD samples in THF under 800 nm (2-photon) excitation and 400 nm excitation. Under the assumption of insignificant pump attenuation, $\beta = P(\kappa\alpha/I_o)$ where β is the two photon cross section in cm^4 s $photon^{-1}$ (10^{50} GM), κ is the ratio of PL counts obtained under 800 and 400 nm excitation, I_o is the intensity of the 800 nm light in photons cm^{-2} s^{-1}, α is the linear absorption cross section at 400 nm and P is the ratio of excitation power at 400 nm to the excitation power at 800 nm. The 800 nm excitation was performed using 250 fs pulses with a repetition rate of 250 kHz. Measurements were performed at varying 800 nm fluences, and the error bars represent the standard deviation across various measurements. Background emission observed during 800 nm excitation was subtracted. Sample degradation was avoided by stirring.

The two-photon cross section of the bare NQDs ($1.3 \pm 0.2 \times 10^4$ GM) was obtained by using a linear absorption cross section of 3×10^{-15} cm^2 at 400 nm. The linear cross section is obtained by fitting the early time transient saturation behavior of the band-edge (1S) excitonic feature to a Poisson distribution function.

Structural Characterization. TEM images were obtained by using JEOL 2010 transmission electron microscope operating at 200 kV. TEM samples were prepared by casting 3 μL of dilute sample solution on carbon-coated copper TEM grids.

Spectroscopic Characterization. Optical absorption spectra were collected on a Cary 5000 UV/vis/NIR spectrophotometer from solutions in 1 cm path length quartz cuvettes. Static PL spectra were collected on a Jobin-Yvon (Horiba) Fluorolog from dilute solutions (OD < 0.1 at the excitation wavelength) in 1 cm path length quartz cuvettes. NP and NQD concentrations were determined from static absorption spectra, using optical absorption cross sections estimated by considering AuNRs as ellipsoids, according to published methods[39,40] as described in the text. NQD cross sections were determined from published literature[43,54−56] or estimated from band edge saturation data in transient absorption experiments.

Conflict of Interest: The authors declare no competing financial interest.

Acknowledgment. L.L., V.I.K., and J.M.P. were supported by the Center for Advanced Solar Photophysics, an Energy Frontier Research Center funded by the U.S. Department of Energy (DOE), Office of Science, Office of Basic Energy Sciences (BES). B.P.K., A.P. and W.K.B. were supported by the Los Alamos National Laboratory Directed Research and Development (LDRD) Program. Q.L. and H.L. were supported by the New Mexico Consortium and Los Alamos National Laboratory.

Supporting Information Available: Additional TEM images; absorption, PL and PL excitation spectra. This material is available free of charge *via* the Internet at http://pubs.acs.org.

REFERENCES AND NOTES

1. Lee, D. C.; Robel, I.; Pietryga, J. M.; Klimov, V. I. Infrared-Active Heterostructured Nanocrystals with Ultra Long Carrier Lifetimes. *J. Am. Chem. Soc.* **2010**, *132*, 9960–9962.
2. Lee, J.-S.; Shevchenko, E. V.; Talapin, D. V. Au−Pbs Core−Shell Nanocrystals: Plasmonic Absorption Enhancement and Electrical Doping *via* Intra-particle Charge Transfer. *J. Am. Chem. Soc.* **2008**, *130*, 9673–9675.
3. Shimizu, K. T.; Woo, W. K.; Fisher, B. R.; Eisler, H. J.; Bawendi, M. G. Surface-Enhanced Emission from Single Semiconductor Nanocrystals. *Phys. Rev. Lett.* **2002**, *89*, 117401.
4. Willingham, B.; Link, S. Energy Transport in Metal Nanoparticle Chains *via* Sub-radiant Plasmon Modes. *Opt. Express* **2011**, *19*, 6450–6461.
5. Klimov, V. I.; Mikhailovsky, A. A.; Xu, S.; Malko, A.; Hollingsworth, J. A.; Leatherdale, C. A.; Eisler, H. J.; Bawendi, M. G. Optical Gain and Stimulated Emission in Nanocrystal Quantum Dots. *Science* **2000**, *290*, 314–317.
6. Noginov, M. A.; Zhu, G.; Belgrave, A. M.; Bakker, R.; Shalaev, V. M.; Narimanov, E. E.; Stout, S.; Herz, E.; Suteewong, T.; Wiesner, U. Demonstration of a Spaser-Based Nanolaser. *Nature* **2009**, *460*, 1110–U68.
7. Song, J.-H.; Atay, T.; Shi, S.; Urabe, H.; Nurmikko, A. V. Large Enhancement of Fluorescence Efficiency from Cdse/Zns Quantum Dots Induced by Resonant Coupling to Spatially Controlled Surface Plasmons. *Nano Lett.* **2005**, *5*, 1557–1561.
8. Atwater, H. A.; Polman, A. Plasmonics for Improved Photovoltaic Devices. *Nat. Mater.* **2010**, *9*, 205–213.
9. Brown, M. D.; Suteewong, T.; Kumar, R. S. S.; D'Innocenzo, V.; Petrozza, A.; Lee, M. M.; Wiesner, U.; Snaith, H. J. Plasmonic Dye-Sensitized Solar Cells Using Core−Shell Metal−Insulator Nanoparticles. *Nano Lett.* **2010**, *11*, 438–445.
10. Albrecht, M. G.; Creighton, J. A. Anomalously Intense Raman-Spectra of Pyridine at a Silver Electrode. *J. Am. Chem. Soc.* **1977**, *99*, 5215–5217.
11. Fleischmann, M.; Hendra, P. J.; McQuilla, A. J. Raman Spectra of Pyridine Adsorbed at a Silver Electrode. *Chem. Phys. Lett.* **1974**, *26*, 163–166.
12. Jeanmaire, D. L.; Vanduyne, R. P. Resonance Raman Spectroelectrochemistry. 2. Scattering Spectroscopy Accompanying Excitation of Lowest B-2(1u) Excited-State of Tetracyanoquinodimethane Anion Radical. *J. Am. Chem. Soc.* **1976**, *98*, 4029–4033.
13. Medintz, I. L.; Stewart, M. H.; Trammell, S. A.; Susumu, K.; Delehanty, J. B.; Mei, B. C.; Melinger, J. S.; Blanco-Canosa, J. B.; Dawson, P. E.; Mattoussi, H. Quantum-Dot/Dopamine Bioconjugates Function as Redox Coupled Assemblies for *in Vitro* and Intracellular pH Sensing. *Nat. Mater.* **2010**, *9*, 676–684.
14. Govorov, A. O.; Bryant, G. W.; Zhang, W.; Skeini, T.; Lee, J.; Kotov, N. A.; Slocik, J. M.; Naik, R. R. Exciton−Plasmon Interaction and Hybrid Excitons in Semiconductor−Metal Nanoparticle Assemblies. *Nano Lett.* **2006**, *6*, 984–994.
15. Liu, N.; Prall, B. S.; Klimov, V. I. Hybrid Gold/Silica/Nanocrystal−Quantum-Dot Superstructures: Synthesis and Analysis of Semiconductor−Metal Interactions. *J. Am. Chem. Soc.* **2006**, *128*, 15362–15363.
16. Vasa, P.; Pomraenke, R.; Schwieger, S.; Mazur, Y. I.; Kunets, V.; Srinivasan, P.; Johnson, E.; Kihm, J. E.; Kim, D. S.; Runge, E.; Salamo, G.; Lienau, C. Coherent Exciton−Surface−Plasmon−Polariton Interaction in Hybrid Metal−Semiconductor Nanostructures *Phys. Rev. Lett.* **2008**, *101*.
17. Wang, H.; Brandl, D. W.; Nordlander, P.; Halas, N. J. Plasmonic Nanostructures: Artificial Molecules. *Acc. Chem. Res.* **2007**, *40*, 53–62.
18. Anger, P.; Bharadwaj, P.; Novotny, L. Enhancement and Quenching of Single-Molecule Fluorescence *Phys. Rev. Lett.* **2006**, *96*.
19. Durach, M.; Rusina, A.; Klimov, V. I.; Stockman, M. I. Nanoplasmonic Renormalization and Enhancement of Coulomb Interactions *New J. Phys.* **2008**, *10*.
20. Lee, J.; Govorov, A. O.; Kotov, N. A. Nanoparticle Assemblies with Molecular Springs: A Nanoscale Thermometer. *Angew. Chem., Int. Ed.* **2005**, *44*, 7439–7442.
21. Pompa, P. P.; Martiradonna, L; Torre, A. D.; Sala, F. D.; Manna, L; De Vittorio, M.; Calabi, F; Cingolani, R; Rinaldi, R Metal-Enhanced Fluorescence of Colloidal Nanocrystals

with Nanoscale Control. *Nat. Nanotechnol.* **2006**, *1*, 126–130.
22. Zeman, E. J.; Schatz, G. C. An Accurate Electromagnetic Theory Study of Surface Enhancement Factors for Ag, Au, Cu, Li, Na, Al, Ga, in, Zn, and Cd. *J. Phys. Chem.* **1987**, *91*, 634–643.
23. Kulakovich, O.; Strekal, N.; Yaroshevich, A.; Maskevich, S.; Gaponenko, S.; Nabiev, I.; Woggon, U.; Artemyev, M. Enhanced Luminescence of CdSe Quantum Dots on Gold Colloids. *Nano Lett.* **2002**, *2*, 1449–1452.
24. Ma, X.; Tan, H.; Kipp, T.; Mews, A. Fluorescence Enhancement, Blinking Suppression, and Gray States of Individual Semiconductor Nanocrystals Close to Gold Nanoparticles. *Nano Lett.* **2010**, *10*, 4166–4174.
25. Komarala, V. K.; Rakovich, Y. P.; Bradley, A. L.; Byrne, S. J.; Gun'ko, Y. K.; Gaponik, N.; Eychmuller, A. Off-Resonance Surface Plasmon Enhanced Spontaneous Emission from CdTe Quantum Dots. *Appl. Phys. Lett.* **2006**, *89*, 253118.
26. Zhang, J.; Tang, Y.; Lee, K.; Ouyang, M. Nonepitaxial Growth of Hybrid Core−Shell Nanostructures with Large Lattice Mismatches. *Science* **2010**, *327*, 1634–1638.
27. Mokari, T.; Sztrum, C. G.; Salant, A.; Rabani, E.; Banin, U. Formation of Asymmetric One-Sided Metal-Tipped Semiconductor Nanocrystal Dots and Rods. *Nat. Mater.* **2005**, *4*, 855–863.
28. Yang, J.; Elim, H. I.; Zhang, Q.; Lee, J. Y.; Ji, W. Rational Synthesis, Self-Assembly, and Optical Properties of Pbs−Au Heterogeneous Nanostructures *via* Preferential Deposition. *J. Am. Chem. Soc.* **2006**, *128*, 11921–11926.
29. Saunders, A. E.; Popov, I.; Banin, U. Synthesis of Hybrid Cds−Au Colloidal Nanostructures. *J. Phys. Chem. B* **2006**, *110*, 25421–25429.
30. Dukovic, G.; Merkle, M. G.; Nelson, J. H.; Hughes, S. M.; Alivisatos, A. P. Photodeposition of Pt on Colloidal Cds and Cdse/Cds Semiconductor Nanostructures. *Adv. Mater.* **2008**, *20*, 4306–4311.
31. Agarwal, A.; Lilly, G. D.; Govorov, A. O.; Kotov, N. A. Optical Emission and Energy Transfer in Nanoparticle−Nanorod Assemblies: Potential Energy Pump System for Negative Refractive Index Materials. *J. Phys. Chem. C* **2008**, *112*, 18314–18320.
32. Fu, A.; Micheel, C. M.; Cha, J.; Chang, H.; Yang, H.; Alivisatos, A. P. Discrete Nanostructures of Quantum Dots/Au with DNA. *J. Am. Chem. Soc.* **2004**, *126*, 10832–10833.
33. Jun, Y.-w.; Choi, J.-s.; Cheon, J. Shape Control of Semiconductor and Metal Oxide Nanocrystals through Nonhydrolytic Colloidal Routes. *Angew. Chem., Int. Ed.* **2006**, *45*, 3414–3439.
34. Liu, M. Z.; Guyot-Sionnest, P. Synthesis and Optical Characterization of Au/Ag Core/Shell Nanorods. *J. Phys. Chem. B* **2004**, *108*, 5882–5888.
35. Jana, N. R.; Gearheart, L.; Murphy, C. J. Seed-Mediated Growth Approach for Shape-Controlled Synthesis of Spheroidal and Rod-like Gold Nanoparticles Using a Surfactant Template. *Adv. Mater.* **2001**, *13*, 1389–1393.
36. Nikoobakht, B.; El-Sayed, M. A. Preparation and Growth Mechanism of Gold Nanorods (NRS) Using Seed-Mediated Growth Method. *Chem. Mater.* **2003**, *15*, 1957–1962.
37. Liz-Marzán, L. M.; Giersig, M.; Mulvaney, P. Synthesis of Nanosized Gold−Silica Core−Shell Particles. *Langmuir* **1996**, *12*, 4329–4335.
38. Ming, T.; Zhao, L.; Yang, Z.; Chen, H. J.; Sun, L. D.; Wang, J. F.; Yan, C. H. Strong Polarization Dependence of Plasmon-Enhanced Fluorescence on Single Gold Nanorods. *Nano Lett.* **2009**, *9*, 3896–3903.
39. Johnson, P. B.; Christy, R. W. Optical-Constants of Noble-Metals. *Phys. Rev. B* **1972**, *6*, 4370–4379.
40. Bohren, C. F.; R.Huffman, D. *Absorption and Scattering of Light by Small Particles*; Wiley: New York, 1998.
41. Pietryga, J. M.; Werder, D. J.; Williams, D. J.; Casson, J. L.; Schaller, R. D.; Klimov, V. I.; Hollingsworth, J. A. Utilizing the Lability of Lead Selenide to Produce Heterostructured Nanocrystals with Bright, Stable Infrared Emission. *J. Am. Chem. Soc.* **2008**, *130*, 4879–4885.
42. Dabbousi, B. O.; Rodriguez-Viejo, J.; Mikulec, F. V.; Heine, J. R.; Mattoussi, H.; Ober, R.; Jensen, K. F.; Bawendi, M. G. (CdSe)ZnS Core−Shell Quantum Dots: Synthesis and Characterization of a Size Series of Highly Luminescent Nanocrystallites. *J. Phys. Chem. B* **1997**, *101*, 9463–9475.
43. Li, L. A.; Pandey, A.; Werder, D. J.; Khanal, B. P.; Pietryga, J. M.; Klimov, V. I. Efficient Synthesis of Highly Luminescent Copper Indium Sulfide-Based Core/Shell Nanocrystals with Surprisingly Long-Lived Emission. *J. Am. Chem. Soc.* **2011**, *133*, 1176–1179.
44. Pandey, A.; Guyot-Sionnest, P. Intraband Spectroscopy and Band Offsets of Colloidal II−VI Core/Shell Structures. *J. Chem. Phys.* **2007**, *127*, 104710.
45. Pietryga, J. M.; Schaller, R. D.; Werder, D.; Stewart, M. H.; Klimov, V. I.; Hollingsworth, J. A. Pushing the Band Gap Envelope: Mid-infrared Emitting Colloidal PbSe Quantum Dots. *J. Am. Chem. Soc.* **2004**, *126*, 11752–11753.
46. Tsung, C. K.; Kou, X. S.; Shi, Q. H.; Zhang, J. P.; Yeung, M. H.; Wang, J. F.; Stucky, G. D. Selective Shortening of Single-Crystalline Gold Nanorods by Mild Oxidation. *J. Am. Chem. Soc.* **2006**, *128*, 5352–5353.
47. Khanal, B. P.; Zubarev, E. R. Purification of High Aspect Ratio Gold Nanorods: Complete Removal of Platelets. *J. Am. Chem. Soc.* **2008**, *130*, 12634–+.
48. Khanal, B. P.; Zubarev, E. R. Rings of Nanorods. *Angew. Chem., Int. Ed.* **2007**, *46*, 2195–2198.
49. Schweikhard, V.; Grubisic, A.; Baker, T. A.; Thomann, I.; Nesbitt, D. J. Polarization-Dependent Scanning Photoionization Microscopy: Ultrafast Plasmon-Mediated Electron Ejection Dynamics in Single Au Nanorods. *ACS Nano* **2011**, *5*, 3724–3735.
50. Larson, D. R.; Zipfel, W. R.; Williams, R. M.; Clark, S. W.; Bruchez, M. P.; Wise, F. W.; Webb, W. W. Water-Soluble Quantum Dots for Multiphoton Fluorescence Imaging *in Vivo*. *Science* **2003**, *300*, 1434–1436.
51. Denk, W.; Strickler, J.; Webb, W. Two-Photon Laser Scanning Fluorescence Microscopy. *Science* **1990**, *248*, 73–76.
52. Lima, I. T.; Marinov, V. R. Volumetric Display Based on Two-Photon Absorption in Quantum Dot Dispersions. *J. Disp. Technol.* **2010**, *6*, 221–228.
53. Li, X. P.; Embden, J.; Chon, J. W. M.; Gu, M. Enhanced Two-Photon Absorption of CdS Nanocrystal Rods. *Appl. Phys. Lett.* **2009**, *94*, 103117.
54. Moreels, I.; Lambert, K.; De Muynck, D.; Vanhaecke, F.; Poelman, D.; Martins, J. C.; Allan, G.; Hens, Z. Composition and Size-Dependent Extinction Coefficient of Colloidal PbSe Quantum Dots. *Chem. Mater.* **2007**, *19*, 6101–6106.
55. Moreels, I.; Lambert, K.; Smeets, D.; De Muynck, D.; Nollet, T.; Martins, J. C.; Vanhaecke, F.; Vantomme, A.; Delerue, C.; Allan, G.; Hens, Z. Size-Dependent Optical Properties of Colloidal PbS Quantum Dots. *ACS Nano* **2009**, *3*, 3023–3030.
56. Yu, W. W.; Qu, L. H.; Guo, W. Z.; Peng, X. G. Experimental Determination of the Extinction Coefficient of CdTe, CdSe, and CdS Nanocrystals. *Chem. Mater.* **2003**, *15*, 2854–2860.